

Algorithm for HF Radar Vector Current Measurements

LEI LIU*, XIONGBIN WU, FENG CHENG, SHAOLIN YANG and HENGYU KE

School of Electronic Information, Wuhan University, Wuhan, Hubei 430079, P.R. China

(Received 22 July 2005; in revised form 29 August 2006; accepted 2 September 2006)

A new algorithm is proposed, called the stream function method (SFM) for producing vector current maps from radial data measured by dual-site high frequency surface wave radar (HFSWR). In SFM, a scalar stream function is constructed under some oceanographic assumptions. The function describes the two-dimensional (2-D) ocean surface water motion and is used to obtain the distribution of vector currents. The performance of SFM is evaluated using simulated radial data, which demonstrates that SFM has advantages over typical vectorial combination methods (VCM) both in error acceptance and robustness, and excels another method based on least-squares fitting (LSF) in recovering the complicated current models. Furthermore, SFM is capable of providing the total currents based on radials from single-site radar. We also test the assumptions of horizontal non-divergence in the simulation. The new algorithm is applied to the field experiment data of Wuhan University's ocean state measuring and analyzing radar (OSMAR), collected in the coastal East China Sea during April 11–17, 2004. Quantitative comparisons are given between radar results by three current algorithms and *in-situ* current meter measurements. Preliminary analysis of the vertical current shear is given based on the current meter measurements.

Keywords:

- HFSWR,
- ocean surface current,
- dual-site,
- stream function,
- OSMAR.

1. Introduction

HFSWR measures ocean surface currents from the Doppler shift of the Bragg-resonant echoes. The Bragg scattering of the HF surface wave involves ocean waves with a wavelength of one half the electromagnetic (EM) wavelength, traveling toward or away from the radar (Barrick, 1972; Teague *et al.*, 1977). HFSWR systems provide valuable information about surface currents, particularly the character of circulation patterns, trends, and relative magnitudes of currents. At the same time, the amplitudes and variations of HFSWR currents can be very erroneous, the magnitudes of errors at times approaching the order of the currents (Lewis *et al.*, 1998). Lipa and Barrick (1983) showed that the sources of uncertainties in CODAR/SeaSonde measurements of radial velocity include statistical uncertainties, systematic errors and errors/simplifications in the analysis. Paduan and Shulman (2004) stated that the largest source of error or bias in every HF radar is introduced when determining the bearing angle to the ocean echo source. Thus, care must be taken in the use of such observations due to uncertainties in the accuracy of the data.

Typically, one radar provides a radial current map and HF current measurement systems usually employ two or more sites situated tens of kilometers apart, allowing a vector current solution to be obtained by combining measurements from the respective sites (Barrick *et al.*, 1977). Leise (1984) gave a vectorial combination method for dual-site radar, called VCM in this paper. The radials from two radars are linearly interpolated to a common grid and combined directly to get the vector current field. However, the calculation of one velocity component becomes unstable along the baseline or at large distances from the sites, where both sites measure the same radial component; the transverse component cannot be constrained. The analysis of Nadai *et al.* (1999) also showed that the probability distribution of measurement error of the current vector depended on the azimuthal difference of the two radar beams. When the azimuthal difference is smaller than 45° or larger than 135°, the measurement errors of the current vector are much larger than when the azimuthal difference ranges from 45 to 135°. These instabilities are inherent shortcomings of radial measurement in that radial errors are amplified by VCM. The radio wave propagation laboratory (RPL) of Wuhan University, China has been developing the HF radar system OSMAR since 1997. Yang *et al.* (2001) reported the VCM measurements by

* Corresponding author. E-mail: liuleiwhu@hotmail.com

OSMAR along with those by moored current meters at a depth of 2 m. They concluded that the current detecting range of OSMAR dual-site system reached 200 km, and mean absolute errors between radar and current meter measurements for current magnitude and direction were 8.0 cm/s and 8.1°, respectively.

Lipa and Barrick (1983) described another algorithm for total current combination from two or more CODAR radars data based on the least-squares fitting (LSF) method. In that algorithm, the common coverage area of the dual-site radar is divided into radar cells; on each cell the total current is determined by least-squares fitting to the radials by minimizing the sum of the deviations between radial measurements and radially projective values of expected vector current. The uncertainties in the total velocities follow from those in the radials using standard linear error propagation, which includes the effects of radial uncertainties as well as the geometry. The analyses of Lewis *et al.* (1998) indicated that the HF/SWR currents have significant divergences and unrealistic spatial variations of divergence. They calculated the divergence of two adjacent grid cells over a distance of about 2.8 km based on the currents measured by CODAR radars. The results indicated highly variable, large divergences and convergences.

These results suggest that HF/SWR data need additional processing as to minimize errors in the data and to make them more useful for various applications. Since the majority of observations and numerical studies show that surface currents have a divergence of the order of $10^{-6}/s$ or less, the output of HF radar systems could be smoothed, perhaps by fitting the field of currents with horizontal non-divergent (or near-non-divergent) conditions (Lewis *et al.*, 1998). Lipa and Barrick (1983) derived a method, applying the 2-D equation of continuity, to provide total current vectors from single-site CODAR data. Kang (1984) investigated the effects of the Asian Monsoon on ocean currents by means of an analytic solution for barotropic currents driven by a uniform, steady meridional wind in the East China Sea, the South China Sea, and the Yellow Sea, by introducing a stream function in his numerical model. This study proposes a new algorithm for producing vector current maps, the stream function method (SFM). In SFM, a scalar stream function is constructed in a local ocean area from the radial observations of HF radar under the assumption of 2-D non-divergent flow. The function describes the 2-D ocean surface water motion and offers a convenient way to obtain the distribution of vector currents.

The critical problem for SFM is whether the assumptions of 2-D divergence-free flow are satisfied in our study region, the coastal East China Sea. As is well known, horizontal divergence in the ocean usually causes an upward flow of subsurface water, i.e. upwelling. Luo and

Yu (1998) reported upwelling stripes off Fujian and Zhejiang with a width of 40 km or so, and the computed largest upwelling, 1.0×10^{-3} cm/s, occurs between 20 and 30 m, but the upwelling could not reach the sea surface. Numerical simulation of Huang *et al.* (1996) indicated that the upwelling in the coastal areas of the East China Sea could be induced by the influence of a tidal nonlinear effect and the sea bottom topography. Pang *et al.* (2002) analyzed the observed data obtained from East China Sea field measurement in 1994, using evaluation and calculation methods. The conclusion was that there was upwelling with a velocity of 2.6×10^{-3} cm/s near the Changjiang River mouth, but the upwelling could not reach the upper 10 m layer. Generally, the vertical component of flow in the top 1–2 m depth is estimated to be much less than 1.0×10^{-3} cm/s as the vertical velocity is equal to zero at the sea surface. On the other hand, we follow Lewis *et al.* (1998) in the examination our OSMAR radar data. The same phenomena are observed. The divergence of two adjacent grid cells is calculated based on OSMAR total currents produced by the conventional VCM. The magnitude of divergence in two adjacent grid cells is of the order of $10^{-5}/s$. A surface divergence of $1.0 \times 10^{-5}/s$ will result in a vertical velocity of 1.0×10^{-3} cm/s in the top 1 or 2 meters. There are also a number of instances in which the divergences of the two grid cells are relatively large but opposite in sign. For a surface layer that is about 2 m thick, the large but opposite-in-sign divergences over a period of tens of minutes will result in sea level differences between the two grid cells of the order of meters. Hence, it is a tradeoff that the currents are constrained with horizontal non-divergent conditions to smooth the abnormal output of HF radar systems. We investigate the effect when horizontal non-divergence assumptions are not satisfied in the study region in the numerical simulations. The performances of SFM are tested on the simulated data fields that include divergence of O (10^{-6} – $10^{-5}/s$).

In recent years, some methods have been developed for real time assimilation and forecasting of coastal currents based on assimilation of HF radar surface current measurements into a coastal ocean model (Lewis *et al.*, 1998; Lipphardt *et al.*, 2000; Oke *et al.*, 2002; Paduan and Shulman, 2004). In particular, Lipphardt *et al.* (2000) described an horizontal fitting analysis technique based on normal mode analysis (NMA), used to blend HF radar observations with results from a primitive equation model. The main differences between NMA and SFM are the following: (i) The NMA methods are free of assumptions about the surface divergence, which ensure that the velocity field is exactly incompressible in three dimensions by constraining the observed surface currents to sets of vorticity and divergence models. (ii) The NMA methods require no-flow normal conditions at coastal boundaries

and normal flow observations on open boundaries, presenting a challenge for coastal ocean nowcasting. SFM do not require any boundary conditions since stream function expressions can be constructed in the local region based on the radial measurements. (iii) The NMA methods blend the HF radar and numerical model velocities with a spectral approach, so the inconsistency in temporal and spatial resolution of the radar and numerical model should be considered in the data processing. For SFM, a stream function model is introduced in producing total current maps, which is a technique that aids in smoothing the HF radar data that include a relatively large horizontal divergence. On the whole, the SFM algorithm is simple and easy to use; moreover, the computation time is significantly reduced.

SFM is introduced first, including the simplifying assumptions, the theory of stream functions, the numerical techniques, such as the Taylor expansion method (Kesan, 2003) and least-squares fitting in realizing SFM and a discussion of error sources. The performances of SFM, LSF and VCM are evaluated using simulated radial data, which demonstrates that SFM has advantages over the old algorithms. In simulation, the vector currents are known as *a priori* knowledge, from which the radial components are extracted. The vector current data are manipulated in simulation so that the performances of three methods can be investigated with various radial current parameters. The new algorithm is then tested on the OSMAR experiment data, where qualitative comparisons between the outputs of the three method and *in-situ* current meter measurements are conducted.

2. Foundations of SFM

SFM is based on oceanographic stream function theory (Kang, 1984; Kowalik and Murty, 1993). Some numerical techniques are applied to solve the partial differential equation to improve the computational accuracy and robustness.

2.1 Simplifying assumptions

The East China Sea is an epi-continental sea. The whole study region in the coastal sea of Zhejiang province is a shelf region shallower than 70 m, more than 70% of which has a depth of about 60 m. Figure 1 shows a sketch of the depth contours in and around our study region. The locations of two OSMAR sites are indicated by hollow circles with their coverage area indicated by the circular sectors. Moored current meters and wind stations, which provided *in-situ* measurements, were in the radar field of view; their locations are indicated by dots in the figure. The current in the study region is considered to be an irregular, semi-diurnal tidal current, where the M2 tidal current is dominant (30–50 cm/s). The amplitude of the M2 tide is almost 1 m (Guo and Yanagi, 1998). The

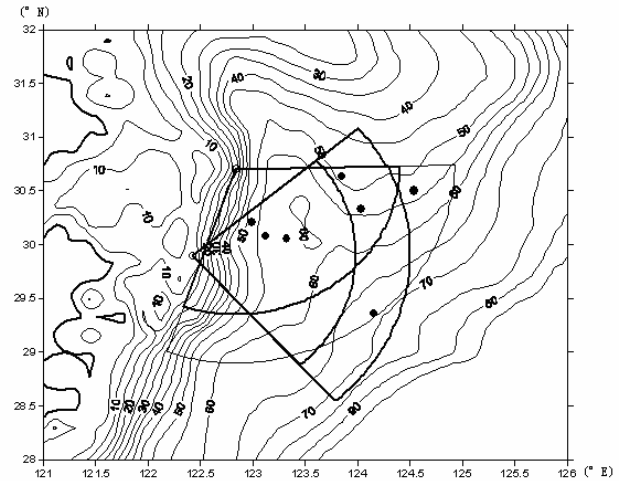


Fig. 1. Depth contours in and around the study region. Locations of two OSMAR sites are indicated by hollow circles with their coverage area indicated by the circular sectors. Mooring current meters and wind stations are indicated by dots.

Changjiang River mouth is located north-west of the study region. Zhu *et al.* (2003) observed diluted water and a plume front off the Changjiang River estuary during August 2000, using CTD, a Multi-parameter Environmental Monitoring System-YSI and other instruments. Figures 2 and 3 (cited from Zhu *et al.*, 2003) show the vertical sections of monthly averaged salinity and temperature in and around the study region in August 2000. They found upwelling was present along the Zhejiang coast, in the north-west outside of our study region. The field observations and numerical simulation experiments have confirmed that significant upwelling exists below 10 m layer from the sea surface in part of the study region. However, it is pointed out that the vertical motion cannot reach the surface layer (Huang *et al.*, 1996; Luo and Yu, 1998; Pang *et al.*, 2002).

Generally, a magnitude of surface divergence in the ocean much larger than $10^{-6}/s$ is not expected. The analyses of Lewis *et al.* (1998) indicated that the HF radar currents had significant divergences and unrealistic spatial variations of divergence. On examination of our OSMAR radar data, we find the same phenomena. The divergence of two adjacent grid cells is calculated based on OSMAR total currents produced by the conventional VCM algorithm during the field experiment. The radar cell spacing is 5 km and the time step is 10 minutes. Figure 4 shows two examples of our calculation results. One pair of grid cells is located in the upwelling stripes observed by Luo and Yu (1998) and Huang *et al.* (1996), while another pair is not. This indicates that the magnitude of diver-

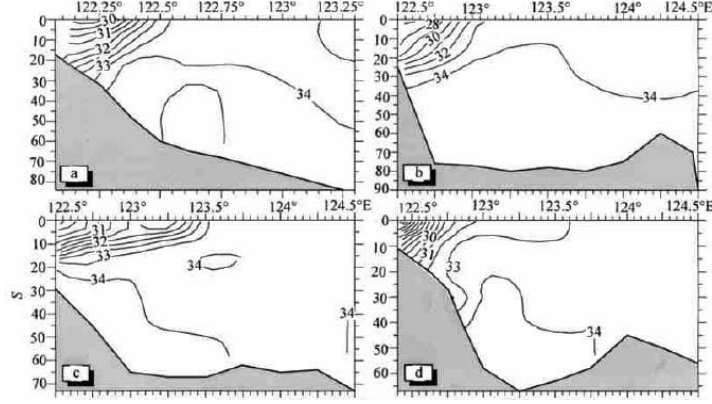


Fig. 2. Vertical sections of average salinity along (a) Section 29°N; (b) Section 30°N; (c) Section 30.5°N; (d) Section 31°N in August 2000 (cited from Zhu *et al.*, 2003).

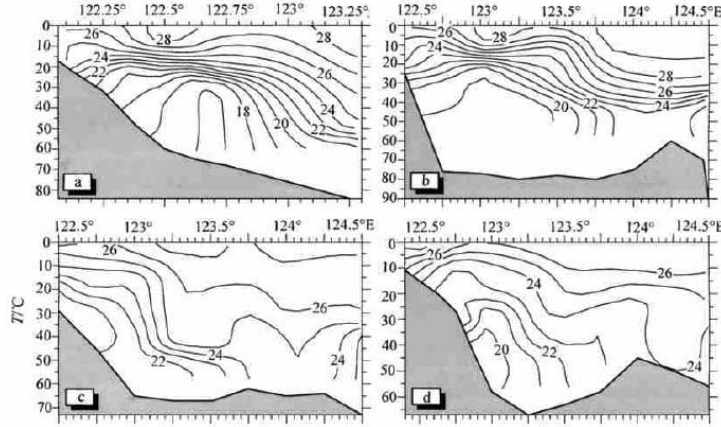


Fig. 3. Vertical sections of average temperature along (a) Section 29°N; (b) Section 30°N; (c) Section 30.5°N; (d) Section 31°N in August 2000 (cited from Zhu *et al.*, 2003).

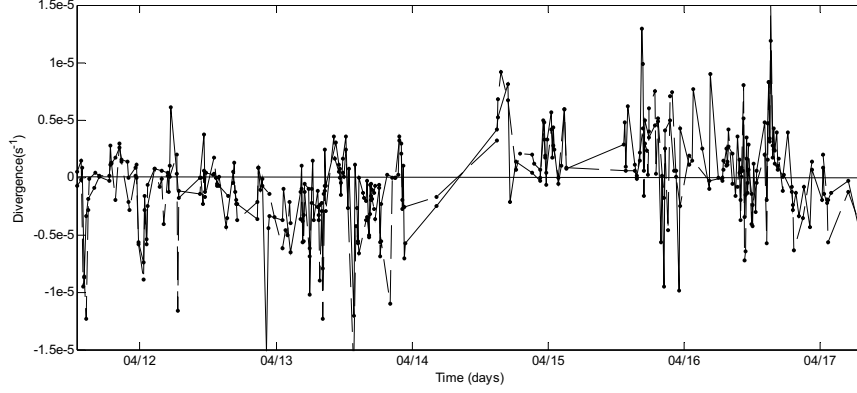
gence of two adjacent grid cells is much larger than $10^{-6}/s$. The 3-D incompressibility condition is

$$\nabla \cdot \vec{V} = \frac{\partial u}{\partial x} + \frac{\partial v}{\partial y} + \frac{\partial w}{\partial z} = 0 \quad (1)$$

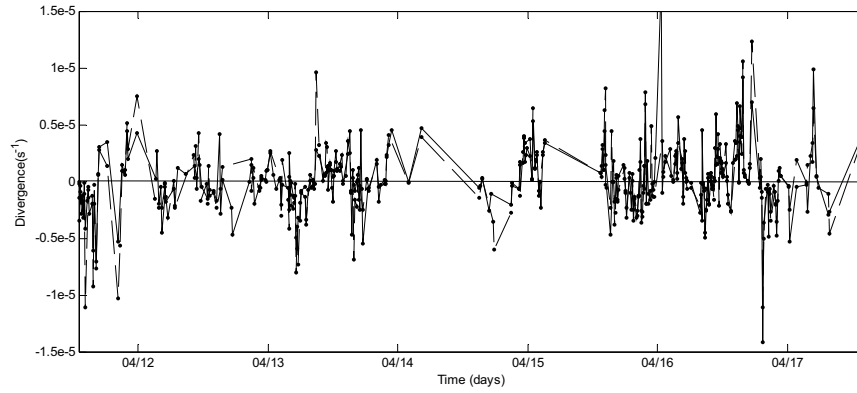
where \vec{V} is vector velocity in the surface layer, u , v and w are three velocity components in the x (east), y (north) and z (upward) directions, respectively. If w is equal to zero at the sea surface, surface divergence of $1.0 \times 10^{-5}/s$ will result in a vertical velocity of 1.0×10^{-3} cm/s in the top 1 or 2 meters, which is comparable to the largest upwelling velocity occurring between 20 and 30 m; while Luo and Yu (1998) proved that the largest upwelling could not reach the top 10 meter layer. Moreover, there are a number of instances in which the divergences of the

two grid cells are relatively large but opposite in sign. For a surface layer that is 1 or 2 m thick, the large but opposite-in-sign divergences over a period of tens of minutes will result in sea level differences between the two grid cells of the order of meters. The same characteristics of surface divergence are observed for the two pairs in the graphs. This indicates that the upwelling in the subsurface water has no significant relations with the surface divergence derived from the HF radar data; or perhaps such relations cannot be manifested in the inaccurate observation data.

Since the majority of observations and numerical studies show that surface currents have a divergence of the order of $10^{-6}/s$ or less, we attempt to smooth the HFSWR data by fitting the field of currents with horizontal non-divergent conditions. In this study, we assume a horizontally non-divergent flow existing in the sea sur-



(a)



(b)

Fig. 4. Time histories of divergence based on the OSMAR current data from two adjacent grid cells at the coastal East China Sea. (a) Solid line: 123°00'00" E, 30°00'00" N; dashed line: 123°03'00" E, 30°00'00" N. (b) Solid line: 123°30'00" E, 30°00'00" N; dashed line: 123°33'00" E, 30°00'00" N.

face layer which HFSWR is able to detect, so Eq. (1) is simplified as

$$\frac{\partial u}{\partial x} + \frac{\partial v}{\partial y} = 0. \quad (2)$$

2.2 Basic principles

Vertically polarized HF radio waves propagating at grazing incidence (i.e. surface wave propagation) are scattered in a resonant interaction with the gravity waves. Techniques have been developed to measure ocean currents in the upper 1–2 m of the ocean surface using HFSWR. As the first-order scattering mechanism is highly selective in terms of the direction of wave propagation, i.e. only those ocean waves that are traveling toward or away from the radar contribute appreciable energy to the first-order echo, a single HF radar can measure the component of ocean current in the direction of the radar site,

which is expressed as

$$V_r = u \cos \theta + v \sin \theta, \quad (3)$$

where V_r is the radial velocity measured by HF radar, θ is the corresponding azimuth angle in polar coordinates.

The 2-D divergence-free ocean water flow may be represented graphically by a flow net, a set of orthogonal streamlines. The streamlines are the loci of points with identical values of the stream function $\psi(x, y)$. A stream function is a general function that describes incompressible flow which may be viscous and/or rotational. In the horizontal plane the flow is along the level curves of the function, i.e. the level curves are the streamlines of the flow. The field of the stream function ψ provides a very general description of oceanic water motion, which gives the components u, v of fluid velocity in the x, y plane as follows:

$$u = -\frac{\partial\psi}{\partial y}, \quad v = \frac{\partial\psi}{\partial x}. \quad (4)$$

The advantage of this equation is that it is easier to find boundary conditions for ψ that are physically correct. Since the ocean is bounded with coasts, and water can neither accumulate near the coast nor cross it, the streamline near the shore will be parallel to it. Since the isolines of ψ are streamlines, the value of ψ should not vary along the shore. In other words, the shoreline is a streamline.

Substituting (4) into (3), it is rewritten in Cartesian coordinates

$$V_r = \frac{1}{\sqrt{x^2 + y^2}} \left(y \frac{\partial\psi}{\partial x} - x \frac{\partial\psi}{\partial y} \right), \quad (5)$$

which is a linear partial differential equation with $\psi = 0$ as boundary condition along the coastline. The attractions of the stream function formulation are that the incompressibility constraint is automatically satisfied, and there is only one scalar unknown to solve for. After the solution of a partial linearization of the stream function equation on the radar grids has been obtained, the velocity field is recovered by Eq. (4).

In the present work we assume the existence of a stream function for a 2-D ocean current field with a semi-open boundary condition. We should point out that the boundary condition ($\psi = 0$) is convenient in oceanographic applications, but it is not used in the SFM realization. In addition, the area where a stream function can be computed is not the whole radar coverage area, but a patch around a certain range-azimuth cell. The solution of the scalar function $\psi(x, y)$ is described below.

2.3 Approximate ψ solution

As the HF radar radial current $V_r(x, y)$ is discretely distributed in the radar beam coverage, an analytic solution of Eq. (5) seems impractical. Thus only numerical solutions can be realized. For this purpose, the Taylor expansion is applied to obtain the approximate solution of linear partial differential equations under specified associated conditions. The method first replaces the unknown by truncated Taylor series with unknown Taylor coefficients around a point (x_0, y_0) . Then $V_r(x, y)$ near (x_0, y_0) are used as measurements to fix the unknowns by means of the least-squares method. In this way, the partial differential equations will be converted to a set of linear algebraic equations.

Assume that stream function $\psi(x, y)$ has partial derivatives until degree $N + 1$ on an interval $a \leq x, y \leq b$, centered in a point (x_0, y_0) ; its Taylor expression in that area is

$$\begin{aligned} \psi(x, y) = & \psi(x_0, y_0) + \left[(x - x_0) \frac{\partial}{\partial x} + (y - y_0) \frac{\partial}{\partial y} \right] \psi(x_0, y_0) \\ & + \frac{1}{2!} \left[(x - x_0) \frac{\partial}{\partial x} + (y - y_0) \frac{\partial}{\partial y} \right]^2 \psi(x_0, y_0) + \dots \\ & + \frac{1}{N!} \left[(x - x_0) \frac{\partial}{\partial x} + (y - y_0) \frac{\partial}{\partial y} \right]^N \psi(x_0, y_0) \\ & + \frac{1}{(N+1)!} \left[(x - x_0) \frac{\partial}{\partial x} + (y - y_0) \frac{\partial}{\partial y} \right]^{N+1} \\ & \cdot \psi(\lambda x + (1-\lambda)x_0, \lambda y + (1-\lambda)y_0) \quad (0 < \lambda < 1). \quad (6) \end{aligned}$$

For a well-developed sea surface, the N degree approximate expression of Eq. (6) is

$$\psi(x, y) = \sum_{n=0}^N \frac{1}{n!} \left[(x - x_0) \frac{\partial}{\partial x} + (y - y_0) \frac{\partial}{\partial y} \right]^n \psi(x_0, y_0), \quad (7)$$

with truncation error

$$\begin{aligned} R = & \frac{1}{(N+1)!} \left[(x - x_0) \frac{\partial}{\partial x} + (y - y_0) \frac{\partial}{\partial y} \right]^{N+1} \\ & \cdot \psi(\lambda x + (1-\lambda)x_0, \lambda y + (1-\lambda)y_0) \quad (0 < \lambda < 1). \end{aligned}$$

In Eqs. (6) and (7), item $[(x - x_0)\partial/\partial x + (y - y_0)\partial/\partial y]^n \psi(x_0, y_0)$ is the total differential of degree n of $\psi(x, y)$ at point (x_0, y_0) , expressed as

$$\begin{aligned} & \left[(x - x_0) \frac{\partial}{\partial x} + (y - y_0) \frac{\partial}{\partial y} \right]^n \psi(x_0, y_0) \\ & = \sum_{k=0}^n C_n^k \frac{\partial^n \psi(x_0, y_0)}{\partial x^k \partial y^{n-k}} (x - x_0)^k (y - y_0)^{n-k} \\ & = \sum_{k=0}^n \frac{n!}{k!(n-k)!} \frac{\partial^n \psi(x_0, y_0)}{\partial x^k \partial y^{n-k}} (x - x_0)^k (y - y_0)^{n-k}. \quad (8) \end{aligned}$$

Substituting Eq. (8) into (7) one obtains

$$\psi(x, y) = \sum_{n=0}^N \sum_{k=0}^n \frac{1}{k!(n-k)!} \frac{\partial^n \psi(x_0, y_0)}{\partial x^k \partial y^{n-k}} (x - x_0)^k (y - y_0)^{n-k}. \quad (9)$$

Let $r = k, s = n - k, f^{(r,s)}(x_0, y_0) = (\partial^{r+s} \psi(x_0, y_0)) / (\partial x^r \partial y^s)$, Eq. (9) is now rewritten as

$$\psi(x, y) = \sum_{r=0}^N \sum_{s=0}^{N-r} \frac{1}{r! \cdot s!} f^{(r,s)}(x_0, y_0) (x - x_0)^r (y - y_0)^s, \quad (10)$$

which is a Taylor polynomial of degree N at $(x, y) = (x_0, y_0)$, where $1/(r! \cdot s!) f^{(r,s)}(x_0, y_0)$, $r, s = 0, 1, \dots, N$ are the coefficients to be determined. The number of unknown Taylor coefficients is controlled by polynomial index N . Larger N corresponds to more radar cells included in calculation of the approximate stream function for the given area. The vector current results may have fewer local truncation errors but they may also be more sensitive to radial measurement error (which will be discussed in the next subsection). Smaller N has the opposite effects. Here we assume $(x_0, y_0) = (0, 0)$, i.e. the center of the area of interest, and express the coefficients by $\alpha_{r,s} = 1/(r! \cdot s!) f^{(r,s)}(x_0, y_0)$, $r, s = 0, 1, \dots, N$ and seek the solution in the form

$$\psi(x, y) = \sum_{r=0}^N \sum_{s=0}^{N-r} \alpha_{r,s} x^r y^s. \quad (11)$$

Substitution of Eq. (11) into Eq. (5) gives a linear algebraic equation

$$V_r = \frac{1}{\sqrt{x^2 + y^2}} \left[\sum_{r=1}^N \sum_{s=1}^{N-r} a_{r,s} (rx^{r-1}y^{s+1} - sx^{r+1}y^{s-1}) + \sum_{r=1}^N a_{r,0} rx^{r-1} - \sum_{s=1}^N a_{0,s} sxy^{s-1} \right]. \quad (12)$$

$1/2(N^2 + 3N)$ unknown Taylor coefficients are included in Eq. (12), meaning that $1/2(N^2 + 3N)$ radials in the area considered are needed to form a linear equation system and determine the solution. However, HF radar measurements over the past several years have revealed that errors exist in estimation of the radial velocities. In order to smooth the effects of noisy radials and seek a more accurate stream function expression, more than $1/2(N^2 + 3N)$ radial samples should be taken into consideration. Assume that M ($M > 1/2(N^2 + 3N)$) radial currents are obtained in an area of radar coverage, put these radial currents in a vector, $\mathbf{V}_r = (V_{r1}, V_{r2}, \dots, V_{rM})^T$, with $\mathbf{x} = (x_1, x_2, \dots, x_M)^T$ and $\mathbf{y} = (y_1, y_2, \dots, y_M)^T$ being the corresponding coordinate vectors. Let $\boldsymbol{\alpha} = (\alpha_{1,1}, \dots, \alpha_{1,N-1}, \alpha_{2,1}, \dots, \alpha_{2,N-2}, \dots, \alpha_{N-1,1}, \alpha_{1,0}, \dots, \alpha_{N,0}, \alpha_{0,1}, \dots, \alpha_{0,N})^T$ be a $1/2(N^2 + 3N)$ column vector to be determined, and let $\mathbf{G} = \{G_{i,j}\}$ be an M by $1/2(N^2 + 3N)$ matrix of coefficients. Linear equation systems are written in matrix form

$$\mathbf{V}_r = \mathbf{G}\boldsymbol{\alpha}. \quad (13)$$

The least-squares solution for the parameters $\alpha_{r,s}$ minimizes the quantity

$$I(\boldsymbol{\alpha}) = (\mathbf{V}_r - \mathbf{G}\boldsymbol{\alpha})^T (\mathbf{V}_r - \mathbf{G}\boldsymbol{\alpha}). \quad (14)$$

This leads to

$$\boldsymbol{\alpha} = (\mathbf{G}^T \mathbf{G})^{-1} \mathbf{G}^T \mathbf{V}_r. \quad (15)$$

Then the u and v in the area of interest can be calculated from Eq. (4)

$$\begin{aligned} u(x, y) &= - \sum_{r=0}^N \sum_{s=1}^{N-r} \alpha_{r,s} s x^r y^{s-1} \\ v(x, y) &= \sum_{r=1}^N \sum_{s=0}^{N-r} \alpha_{r,s} s x^{r-1} y^s. \end{aligned} \quad (16)$$

The total velocity, defined with magnitude V and direction ν , is obtained by combining u and v

$$\begin{aligned} V(x, y) &= \sqrt{u(x, y)^2 + v(x, y)^2} \\ \nu(x, y) &= \tan^{-1}[v(x, y)/u(x, y)]. \end{aligned} \quad (17)$$

2.4 Sources of error

Various sources of error are discussed in this subsection.

1) Truncation limit

The number of unknown Taylor coefficients is controlled by polynomial index N . Estimating N is important. To obtain the best solution of Eq. (5), we must take more terms from the Taylor expansion of functions; that is, the truncation limit N must be chosen sufficiently large. However, too large a number will impact the computational efficiency. On the one hand, the number of radials M is required to be large enough to fit the data involved in the least-squares method, meanwhile increasing the radar coverage cell area correspondingly. On the other hand, we find in the simulation that SFM is not so robust when a stream function of $N > 2$ is constructed for the noisy-added radial currents, i.e. higher order processing is more sensitive to radial sampling error. In this case, high-order least-squares fitting causes computational instability, since the number of coefficients to be determined increases by $1/2(N^2 + 3N)$. Therefore N must be chosen carefully. Generally, HF radar current measurements assume constant velocity over a radar cell. Here we assume the water motion is smooth; the velocity of particles will not change greatly in a limited area. When the truncation limit $N = 2$, the second order stream function is appropri-

ate to describe the complexity of ocean water motion. Uniform or linearly variational current are special cases of the proposed solution. When a more complicated current field is involved, the truncation error must be considered. Truncation limit $N < 3$ is selected in the remainder of this section.

2) Resolution

In data processing, the radar beam coverage area is divided into various radar cells, whose sizes are determined by radar spatial resolution both in range and azimuth. To determine the stream function in a certain radar cell, the radial current measurements in the given radar cell as well as those in surrounding radar cells are all taken into consideration. The number of unknown Taylor coefficients determines how many radar cells are included. The number of cells should be sufficiently larger than the number of Taylor coefficients. Thus, SFM area size is much larger than the radar cell size. In this paper, the local area where a stream function is constructed is about 20 by 20 km on condition that radar parameters are selected such as range resolution 5 km, azimuth resolution of 2.5° and truncation limit $N < 3$. In fact, surface currents are highly variable due to strong influence of local surface wind and wave fields. However, the SFM method assumes a uniform or linear current variation over many radar cells; this process in turn implies a decrease of spatial resolution in the output vector currents map. As for the time scales of the SFM algorithm, the radial current maps are real-time output every 10 minutes for the OSMAR system and SFM vector current results can be obtained almost synchronously if the radial data from two radar site are both available.

3) Radial noise

Our measurements over the past several years have revealed that the greatest source of errors in the vector current mapping using the VCM comes from the errors in estimating the radial velocities. Most uncertainty in these radial vectors is due to spatial and temporal variations of the current field and use of non-optimal analysis parameters (Lipa and Barrick, 1983). Spatial uncertainty results because many different current velocities can be present in the radar scatter patch due to horizontal shear; these velocity values are calculated during analysis and are averaged to produce the output value for that location. This spatial uncertainty usually increases with distance from the radar as the size of the radar scatter patch increases proportionally with range. Uncertainty can also arise from variations in the current velocity field over the duration of the radar measurement, and from assumptions and simplifications that are made during the analysis process.

Now we take into account the measurement errors of radial currents. Assuming observational radial currents \mathbf{V}_r^* have the form of a linear model as

$$\mathbf{V}_r^* = \mathbf{G}\boldsymbol{\alpha} + \mathbf{w}, \quad (18)$$

where \mathbf{w} is a noise vector of M by 1, with zero mean and covariance matrix \mathbf{C} of M by M . The least-squares solution for the parameters $\boldsymbol{\alpha}_{r,s}$ minimizes the quantity

$$I(\boldsymbol{\alpha}) = (\mathbf{V}_r^* - \mathbf{G}\boldsymbol{\alpha})^T (\mathbf{V}_r^* - \mathbf{G}\boldsymbol{\alpha}). \quad (19)$$

This leads to

$$\boldsymbol{\alpha}^* = (\mathbf{G}^T \mathbf{C}^{-1} \mathbf{G})^{-1} \mathbf{G}^T \mathbf{C}^{-1} \mathbf{V}_r^*, \quad (20)$$

and the covariance matrix of $\boldsymbol{\alpha}^*$ is

$$\mathbf{C}_{\boldsymbol{\alpha}^*} = (\mathbf{G}^T \mathbf{C}^{-1} \mathbf{G})^{-1}. \quad (21)$$

The standard deviation in the u and v can be given by Δu and Δv from the formula (21), then the standard deviation of total velocity by linear error propagation is

$$\begin{aligned} \Delta V &= \frac{1}{V} \sqrt{(u\Delta u)^2 + (v\Delta v)^2} \\ \Delta v &= \frac{1}{V^2} \sqrt{(u\Delta u)^2 + (v\Delta v)^2}. \end{aligned} \quad (22)$$

4) Assumption of horizontal non-divergence

The basic assumption of the SFM method is that the ocean current is a horizontally non-divergent flow. If that holds, we can expect that SFM is robust and able to provide quite accurate surface current maps (taking no account of the effect of measurement errors of radial currents). The method considered here seems to be inapplicable in areas where water motion varies rapidly, such as a gulf, channel or some areas where the vertical gradient of ocean water motion in the surface layer is not negligible when upwelling or downwelling occurs.

In order to evaluate the performance of SFM, or any other question regarding the accuracy of HF radar algorithms, some measure of success or ground truth is required. Nadai *et al.* (1999), among others, have made substantial progress in estimating VCM errors through comparison with moored current meter measurements. However, inherent differences between measurements methods and uncertainties in the *in-situ* measurements themselves limit this method of estimating HF radar measurement errors. For instance, taking account of the vertical current shear, HF radar is averaging the currents over a 1 or 2 meter thick layer below the sea surface, whereas the current meter is measuring the currents at the mooring depth. Furthermore, we should bear in mind that part

of the error arises from the temporal and spatial mismatch between the *in-situ* measurement and the 2.5/5 km radar footprint. In the next section we evaluate the performance of the SFM algorithm with various current models including spatial variation, radial errors and horizontal divergence etc. via simulation experiments.

3. Simulations

In this section a computer simulation is used to analyze the errors in HFSWR ocean vector current measurements based on radial data from two radar sites. For simulations, the surface current fields are known, and may be manipulated so that the performance of the methods can be compared over a range of conditions. In particular, using simulated data can help demonstrate the effect of applying the zero horizontal divergence SFM assumption to a data field that includes divergence.

3.1 HFSWR vector current algorithms

Three algorithms for producing vector current maps—an algebraic approach using vectorial combination (VCM) developed by Leise (1984), a numerical method using least-squares fitting (LSF) of Lipa and Barrick (1983) and the new algorithm based on the oceanographic stream function model, SFM—are compared in terms of the effect of variations in radial current input. In VCM, the radials from two radars are linearly interpolated to a common grid and directly combined to obtain vector current fields. Details of VCM can be found in Leise (1984) and Nadai *et al.* (1999). In LSF of Lipa and Barrick (1983), the radial current uncertainties are used as a weighting of the least-squares fit radial current input; they are set to 1 in this study. The radar system parameters used in the simulation are taken from the Wuhan University’s OSMAR system, which operates on a central frequency of 7.5 MHz and is able to detect surface current as far as 200 km, with a range resolution of 2.5 or 5 km and an azimuthally resolution of 2.5°.

3.2 Generation of simulated data

The simulation procedure includes simulating the vector current field, generating radial currents from the given vector current field and comparing the simulated surface currents with those estimated by three methods. We simulate the surface currents at the coastal East China Sea near the Zhoushan Islands, Zhejiang Province. The domain of the vector current model extends from 122.35°E to 124.85°E and from 28.25°N to 31.75°N, which well covers the footprints of two radars, A and B. The geometry is shown in Fig. 5. The local area where a stream function is constructed is about 20 by 20 km; examples are indicated by two boxes in Fig. 5. Such boxes partially overlap each other, so more than one current

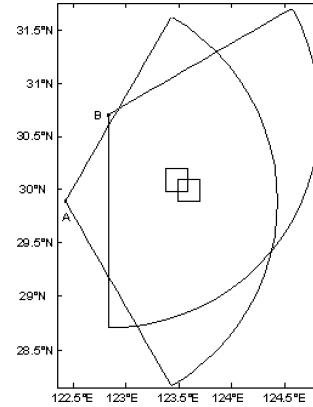


Fig. 5. Radar geometry considered for simulation. Two radar sites A and B are indicated by dots; corresponding radar detection areas are indicated by circular sectors. The little box is an area unit where a stream function is constructed.

velocity result for each grid cell may be engendered from different boxes. For this problem we have included weighting factors in the average of all the available results for each grid cell. For example, the weights could represent a distance averaging or filter processing.

For convenience of expression, we formulate our current models in the Cartesian coordinate system in the plane with the origin (0, 0) at the point 122°E, 30°N. The x axis is eastward, y axis is northward, and their units are km. Current amplitudes of 0–150 cm/s are chosen for the various current models, in the range of current velocities that the HF radar systems are commonly designed to measure. First, vector current fields are simulated to satisfy the 2-D non-divergent condition expressed by Eq. (2), including uniform and non-uniform current fields. Secondly, the Gaussian noises are added to ideal currents so that we can consider the effects of radial errors on the performance of all methods. Finally, data fields having a certain horizontal divergence are combined with the ideal currents in order to investigate the effect of the SFM assumptions. Radial currents are distributed in a grid of range/azimuth cells on the ocean surface. The radial current fields are configured in a circular sector covering 200 km of range and 120° of azimuth, with a range resolution of 5 km and an azimuth resolution of 2.5° for both radar sites. Figure 6 shows examples of the simulated field of uniform current model and the intermediate radial maps extracted from the uniform current field for radar sites A and B, respectively. We should point out that the range resolution and azimuth resolution are set as described above in the algorithm computation, but they have been doubled in illustrations for discerning the radar footprints in this section.

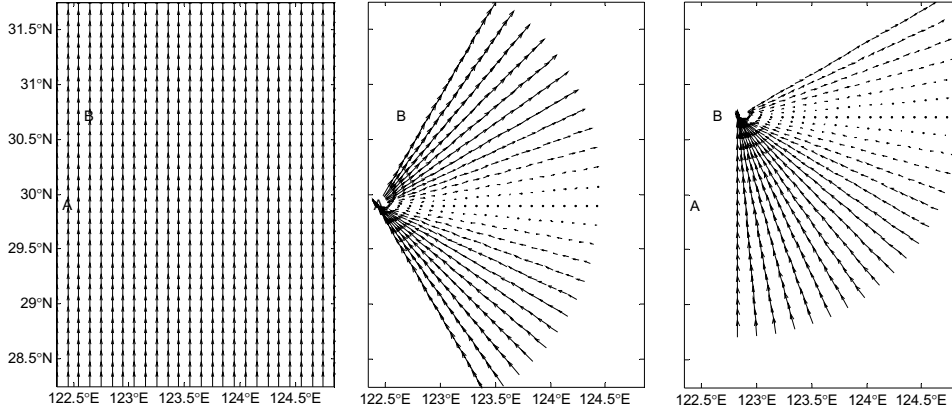


Fig. 6. Results for uniform current model with a simulated uniform current field, the intermediate radial current maps of site A and site B.

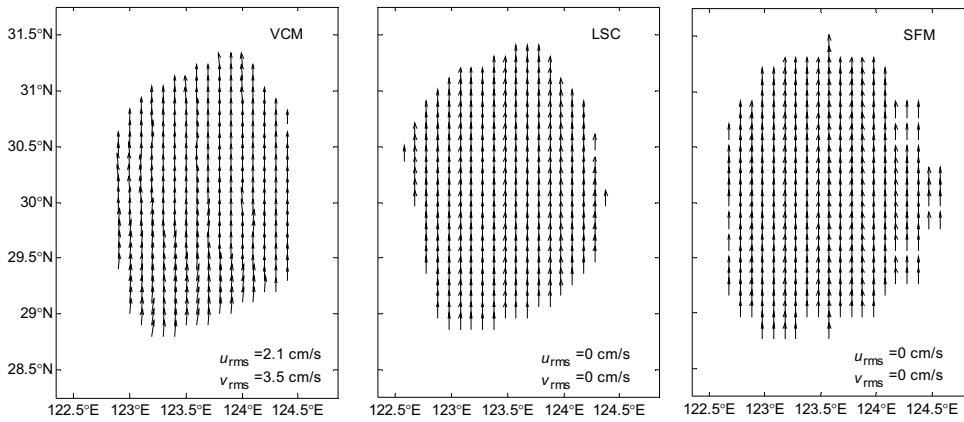


Fig. 7. Vector current maps produced by VCM, LSF and SFM from the intermediate radials.

3.3 Results

The simulation results of three methods under the varying radial current conditions are reported here.

1) Uniform current

A uniform current with an amplitude of 50 cm/s in the direction of due north is used. The radial current data are processed with VCM, LSF and SFM. Figure 7 shows the corresponding vector current results from the three methods. The VCM results have little bias, generally less than the ground truth. As discussed at the beginning of this paper, the linear interpolation is the main cause of the VCM bias. The results show that both the LSF and SFM measurements are nearly equivalent to the simulated vector currents. Moreover, the first-order stream function can describe a uniform current field, which is very easy to implement using the SFM method. The root mean square (RMS) differences between the estimated results of the three methods and the given vector current for all

the radar cells are calculated and shown at the bottom of the corresponding current maps.

2) Sensitivity to errors in radials

In the preceding subsection the intermediate radial currents were extracted from the given vector currents, without adding any errors. However, the greatest source of errors in the vector current mapping using VCM comes from the errors in the estimation of radial velocities. Here we evaluate the effect of radial errors on the results of vector current algorithms, through simulation by adding a Gaussian noise. The given vector current field is still the uniform current with an amplitude of 50 cm/s in the direction of due north. A zero-mean Gaussian noise in current velocity with a SD of 5 cm/s, 10 cm/s and 15 cm/s is added to the intermediate radial maps, respectively. The vector current maps obtained from the radials with a noise SD of 10 cm/s are given in Fig. 8. Table 1 lists the RMS errors of u and v components in different

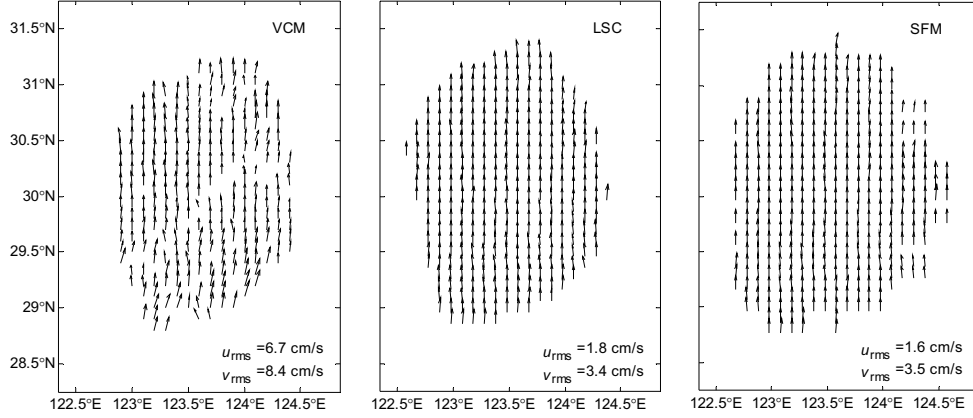


Fig. 8. Results for the uniform current model but with noise of SD 10 cm/s in magnitude added in the radial data.

Table 1. RMS errors for the uniform current model experiment (cm/s).

Method	SD of radial errors							
	0		5		10		15	
	u_{rms}	v_{rms}	u_{rms}	v_{rms}	u_{rms}	v_{rms}	u_{rms}	v_{rms}
VCM	2.1	3.5	4.2	6.6	6.7	8.4	7.9	11
LSF	0	0	1.3	2.6	1.8	3.4	3.9	4.4
SFM	0	0	1.3	2.7	1.6	3.5	2.9	3.7

conditions of radial current input for the uniform current simulation experiment. The LSF- and SFM-derived vector current results are not as accurate as the case when the ideal radials are used. The VCM-derived vector current results appear more affected by the radial current errors and the estimation of the vector current map is worse. The results indicate that the radial current errors do influence the estimation accuracy of each method; LSF and SFM have similar error acceptance capability, but SFM excels LSF in processing radials with a larger noise.

3) Current field spatial variation

We next investigate the case of an ocean surface current field that has spatial variation in current velocity. An example of such a current map is expressed as $u = -2.5 \times 10^{-6}x$ km/s and $v = (2.5y + 500) \times 10^{-6}$ km/s. Such a current field has no horizontal divergence, but varies in both velocity amplitude and direction. The vector currents are derived from the corresponding intermediate and noise-added radial maps, as we do with the uniform current model. Figure 9 shows the resulting vector current maps when a zero-mean Gaussian noise in radial velocity with a SD of 10 cm/s is added. Table 2 lists the RMS errors under different conditions of radial current inputs. It indicates that current fields derived from LSF and SFM remain stay robust after Gaussian noises are added, while those derived from VCM seem disorderly when the SD

of noise increases to 10 cm/s. The RMS errors of SFM-derived results are smaller than those of LSF-derived results in all instances; moreover, only SFM produces the total currents without from the intermediate radials, even in the marginal area where only radial data from one radar are available. It is thought that SFM excels LSF in dealing with the non-uniform current fields that have no horizontal divergence.

4) Effect of horizontal divergence

Here we investigate the effect when horizontal non-divergence assumptions are not satisfied in the study region. In fact, the assumptions are not quite satisfied in the study region, where the M2 tidal current is dominant, and the amplitude of the M2 tide is almost 1 m (Guo and Yanagi, 1998). The continuity equation in a homogeneous and invicid ocean of constant depth, subject to a uniform wind stress is

$$\frac{\partial \eta}{\partial t} + \frac{\partial(H\bar{u})}{\partial x} + \frac{\partial(H\bar{v})}{\partial y} = 0 \quad (23)$$

where \bar{u} and \bar{v} are vertically-averaged velocities in the x (east) and y (north) directions, respectively, η is the sea-level elevation from the sea surface, and H is the depth of the ocean. If the sea elevation is about 1 m (Guo and

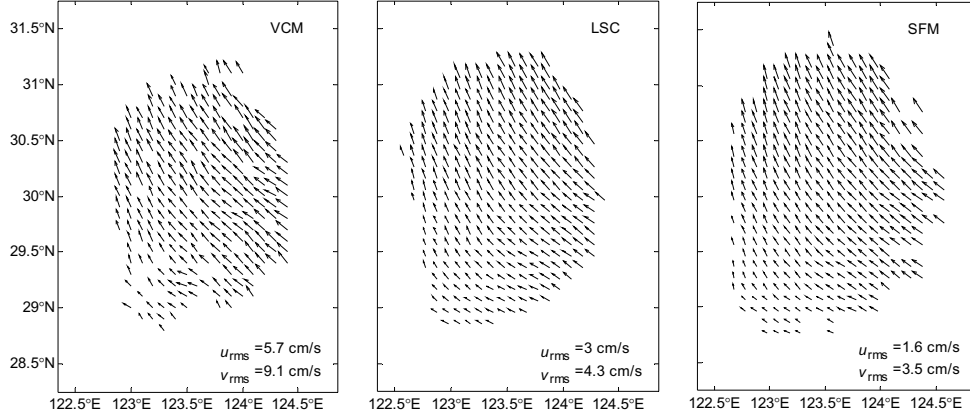


Fig. 9. Vector current maps derived from radial current maps with added noise of SD 10 cm/s in magnitude for current field model with spatial variation.

Table 2. RMS errors for the non-uniform current model experiment (cm/s).

Method	SD of radial errors							
	0		5		10		15	
	u_{rms}	v_{rms}	u_{rms}	v_{rms}	u_{rms}	v_{rms}	u_{rms}	v_{rms}
VCM	1.8	4.9	3.6	7.2	5.7	9.1	7.7	11
LSF	2.2	2.0	2.6	2.2	2.2	3.0	4.1	4.4
SFM	0	0	0.9	1.6	1.6	1.6	3.4	3.0

Table 3. RMS errors for the experiment of current model with a divergence of $10^{-6}/s$ (cm/s).

Method	SD of radial errors							
	0		5		10		15	
	u_{rms}	v_{rms}	u_{rms}	v_{rms}	u_{rms}	v_{rms}	u_{rms}	v_{rms}
VCM	1.5	4.4	3.3	5.5	5.3	8.3	8.1	14
LSF	1.8	1.7	2.6	2.5	2.4	4.5	3.2	4.2
SFM	0.49	0.36	1.1	1.3	3	3.3	3.5	3.1

Yanagi, 1998), the term $\partial\eta/\partial t$ in the continuity equation is estimated to be $O(10^{-5}-10^{-4} \text{ m/s})$. So the term $\partial(H\bar{u})/\partial x + \partial(H\bar{v})/\partial y$ is estimated to be $O(10^{-5}-10^{-4} \text{ m/s})$. Assuming constant depth (60 m) in the study region, the horizontal divergence of vertically averaged velocities $\partial\bar{u}/\partial x + \partial\bar{v}/\partial y$, is $O(10^{-6}-10^{-5}/s)$. Our discussion in Subsection 2.1 indicates that the surface divergence in the top 1–2 m layer is not more than $10^{-5}/s$. Here, the performances of SFM are tested on the simulated data fields that include divergence of $O(10^{-6}-10^{-5}/s)$.

First we simulate a current model having divergence of $10^{-6}/s$, which is considered the superposition of two components, including the non-divergent part (uniform

currents) and a divergent part. For example, the distribution function of u, v velocity components is expressed as $u = -2 \times 10^{-6}x \text{ km/s}$ and $v = (3y + 500) \times 10^{-6} \text{ km/s}$. Table 3 lists the RMS errors under different conditions of radial current inputs for the model with a divergence of $10^{-6}/s$. It is obvious that horizontal divergence does influence the performance of the SFM algorithm, but the bias of SFM-derived results is still smaller than those of the other two methods. Another model tested is described as $u = 2.5 \times 10^{-6}x \text{ km/s}$ and $v = (7.5y + 500) \times 10^{-6} \text{ km/s}$, with a uniform divergence of $10^{-5}/s$. The inverse vector currents using three methods from the corresponding intermediate radial maps are given in Fig. 10. We can see

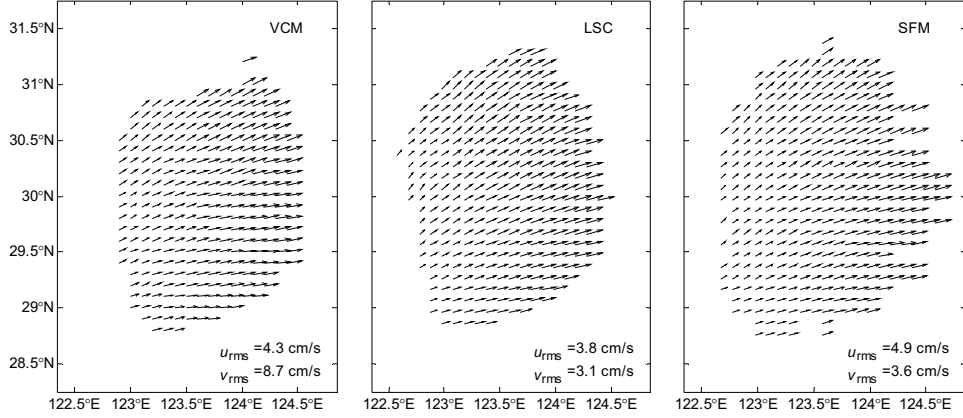


Fig. 10. Vector current maps derived from radial current maps with added noise of SD 10 cm/s in magnitude for current field model with a uniform divergence of $10^{-5}/s$.

Table 4. RMS errors for the experiment of current model with a divergence of $10^{-5}/s$ (cm/s).

Method	SD of radial errors							
	0		5		10		15	
	u_{rms}	v_{rms}	u_{rms}	v_{rms}	u_{rms}	v_{rms}	u_{rms}	v_{rms}
VCM	4.3	8.7	5.8	9.4	10	9.9	13	12
LSF	3.8	3.1	3.9	3.3	4.8	4.6	4.1	4.7
SFM	4.9	3.6	4.9	3.7	5.4	4.8	5.0	4.4

that the horizontal divergence is a great challenge for the SFM method, for the bias of SFM-derived results becomes a little larger than that of LSF-derived results. Table 4 lists the RMS errors under different conditions of radial current inputs for the current model with a divergence of $10^{-5}/s$. The three methods do not perform perfectly in this case. The performance of SFM is very similar to LSF, despite the fact that u_{rms} and v_{rms} are 1.0 and 0.5 cm/s larger, respectively. This is obviously due to the constraints of non-divergence in the SFM method. Though the RMS error of SFM-derived currents is not a simple superposition of RMS errors of the above two components, the errors induced by the divergent component obviously dominate in the current results.

3.4 Conclusion

Some important conclusions from the simulation experiments are the following:

1) SFM and LSF have better error acceptance capability. It is thought that SFM and LSF avoid the errors of VCM connected to the interpolation. Due to the processing of least-squares fitting to the radial data in both methods and the weighted averaging of vector current results in SFM, SFM and LSF smooth the effect of radial observation errors on the vector current results to

a certain degree, while the bias of VCM-derived current results increases rapidly with the increase of radial SD errors in the simulations.

2) SFM excels LSF in processing the complicated current fields. In the LSF method, the current is assumed to be uniform in a local spatial region (in this study, it is set to be as large as the box where a stream function is constructed), while the SFM method is able to show the second order variation of the stream function in this study. Though the current models in the simulation experiments are special examples which are expressed as uniformly or linearly varying functions, it is expected that SFM recovers the spatial variation better than LSF in practical application.

3) SFM has a unique advantage in that its current maps cover a larger sea area in general. It is thought that different data processing between SFM and the two older methods results in a different coverage area: for VCM and LSF, radial currents from two radar sites are combined or fitted for each radar cell, i.e. a vector current is obtained only when a radar cell is illuminated by two radars; for SFM, a vector current field is obtained in a local area covering some radar cells after a scalar stream function is constructed based on the radials falling into that area, so reasonable vector currents are generated in

the marginal area, that is, only if one radar cell is illuminated. In practice, HF radar radials usually do not cover the radar beam uniformly, i.e., there are many gaps in the radial maps, so it is expected that the SFM method can fill the spatial voids as long as one item of radar data is available in the region of interest. It also indicates that SFM is applicable to single-site radar vector current measurements.

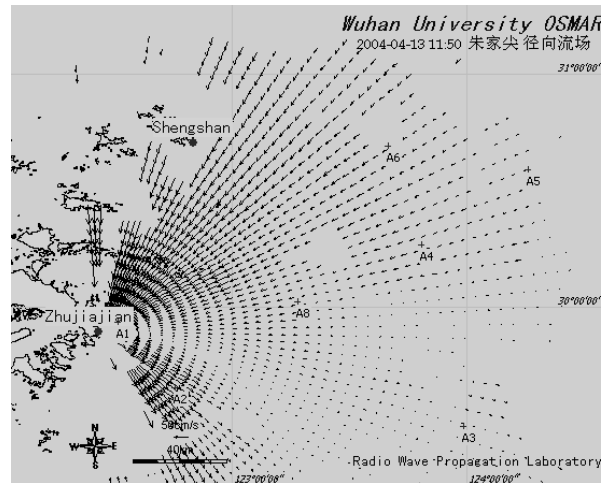
4) As discussed above, a disadvantage of SFM is a decreased computational precision if the horizontal non-divergence assumptions are not well satisfied in the study region. The additional errors caused by the divergent component increase with increasing amplitude of divergence. Compared with the results produced by VCM and LSF, such errors are negligible when the current model contains an added horizontal divergence of $10^{-6}/s$ as input. Though SFM excels VCM, it is put in the shade by LSF when the divergence is on the order of $10^{-5}/s$. Fortunately, so large a divergence, up to $10^{-5}/s$, is seldom observed, either in the study region or in most of the world's oceans. In addition, SFM generally requires a few seconds for a model run on a Pentium 4 machine, while the computation time of the other two methods is less than one second on the same machine.

4. Study of Field Experiment Data

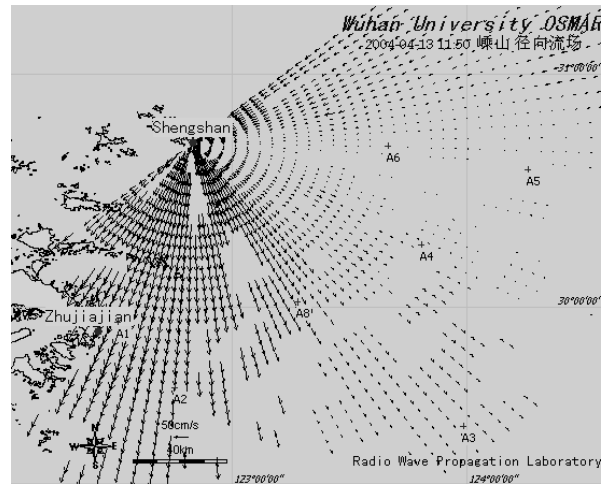
The RPL of Wuhan University has been developing the HFSWR system OSMAR since 1997 in the project "HFSWR Technique in Monitoring Ocean Environment", which receives funding from the National High Technology Research and Development Program of China (the 863 Program). OSMAR is a wide-band radar, adopting a frequency modulated interrupted continuous waveform (FMICW), operating on a centre frequency of 7.5 MHz. The transmitting antenna is a three-element Yagi aerial. The receiving antenna is a beeline array composed of two rows, 13.3 m apart. In each row there are 4 monopoles which are evenly spaced at 8 meters. Radar range and Doppler (or current velocity) resolution are accomplished by double fast-Fourier transforms (double-FFT), and the bearings are determined by the minimum variance method (MVM) or multiple signal classification (MUSIC) algorithm. The OSMAR current data used in this paper are obtained from the MUSIC algorithm (Yang *et al.*, 2001). The radar is able to detect surface current as far as 200 km, and also extract wave and wind with less detection range than that for surface current.

4.1 Radar installation

The RPL has two sets of OSMAR systems with the same specifications. The radar main site is located in Zhujiajian Island and a slave site is located at Shengshan, Zhoushan Islands of Zhejiang Province. From April 11 to 17, 2004, a field experiment was conducted in the East



(a)



(b)

Fig. 11. Radar sites diagram indicated by dots at the shore. Seven ship mooring locations are indicated by crosses. Radial current maps measured by OSMAR at (a) Zhujiajian and (b) Shengshan radar site on 11:50, April 13, 2004 are also shown.

China Sea. The verification tests of OSMAR against traditional marine instruments' *in-situ* measurements were conducted with the collaboration of Wuhan University, Donghai Substation of the State Marine Bureau, the First Marine Research Institute of the State Marine Bureau and China Marine University. A map of the experiment locations is shown in Fig. 11. The locations of two OSMAR sites are indicated by dots at the shore. Seven ship mooring locations, A1–A6 and A8, which provided *in-situ* measurements, were in the radars' common detection area; their positions are indicated in the figure by crosses. Conventional instruments lowered from ships included RCM9

Aanderaa current meter for measuring currents, temperature, conductance and hydraulic pressure, AZF1-II wave gauge for measuring wave height and direction, and XZC5-1 shipping telemetry system for measuring wind velocity and direction. The overall goal of this experiment was to validate the gauge of the ocean surface state parameters measured by OSMAR. Here we only discuss the ocean surface current measurements.

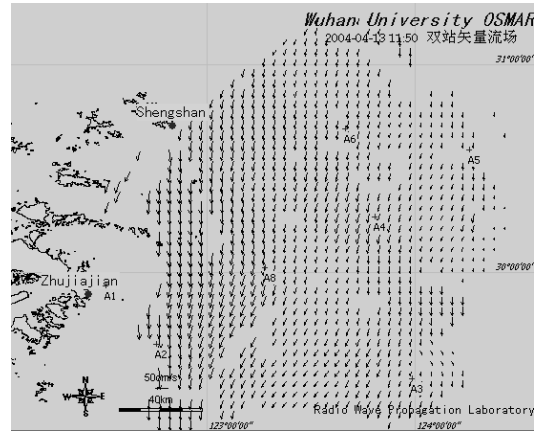
4.2 Current maps

Both OSMARs were operated with the same parameters. The observations were conducted every 10 minutes from April 11 to April 17, 2004. Unfortunately, the main radar was interrupted by a power cut, which lasted for several hours on April 14 and 15, so its data sets were incomplete. Figure 11 also shows examples of radial current maps measured at Zhujiajian and Shengshan, respectively. Both OSAMRs measured the radial current velocities with a directional resolution of 2.5° , range resolution 2.5/5 km, and the arrow marks denote the magnitude and direction of vector currents. The attainable maximum distance for current measurement is strongly affected by the condition of the sea surface, external noise, and the path of the radio waves (Nadai *et al.*, 1997). When sea surface conditions are appropriate and there is little external noise, the OSMAR can measure radial surface current velocities over a distance of 200 km. Under poor surface conditions, however, the maximum distance for radial current measurement becomes less than 100 km. The actual software of the ocean surface current algorithm based on the MUSIC algorithm for the OSMAR system was an improvement over that used in earlier experiments. The amplitude response of the receiving channels was calibrated previously, while the calibration aimed at both amplitude and phase responses in this experiment.

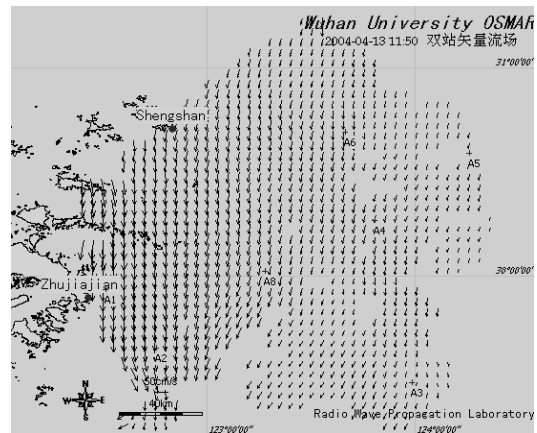
Figure 12 shows examples of vector current maps which are interpolated onto a 2.5 by 2.5 km grid, generated using VCM, LSF and SFM from the dual-site radial maps shown in Fig. 11. It shows good agreement between three results, except that SFM current maps cover a larger sea area in general. Current maps are produced every 10 minutes when the two radars were functioning normally. There are many instances when reasonable vector currents are generated in the marginal area that is illuminated by only one radar using SFM, as discussed in the simulation. The direction of vector field rotates clockwise, changing periodically, a main feature of the semi-diurnal tidal current in the observations area (Guo and Yanagi, 1998).

4.3 Comparisons with current meter measurements

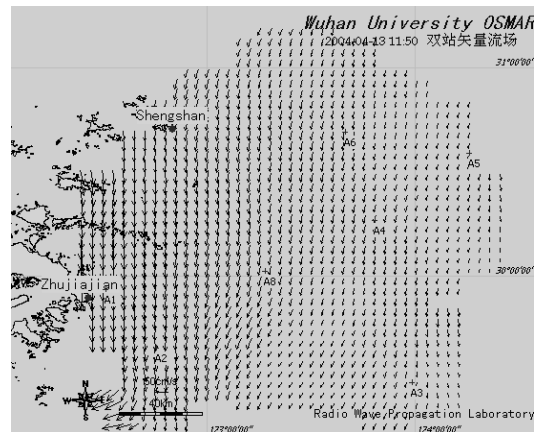
A research ship sailed during the field experiment and moored successively at seven stations where conventional observations were provided in different timeslices.



(a)



(b)



(c)

Fig. 12. Examples of vector currents produced by (a) VCM (b) LSF and (c) SFM.

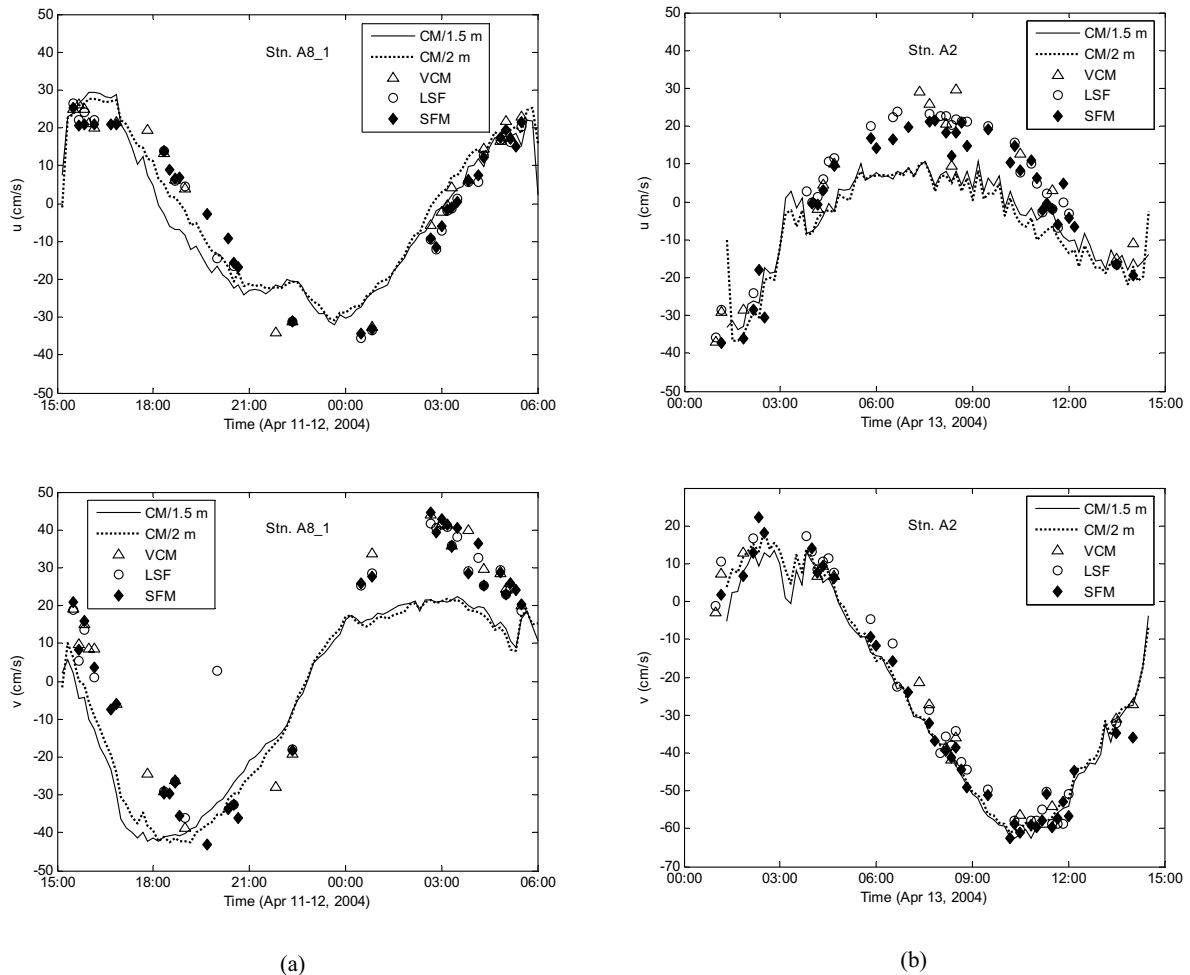
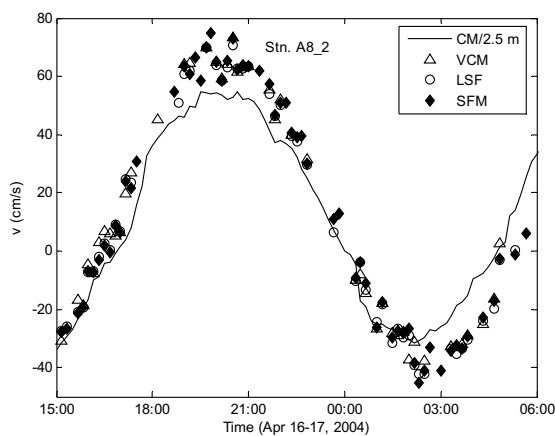
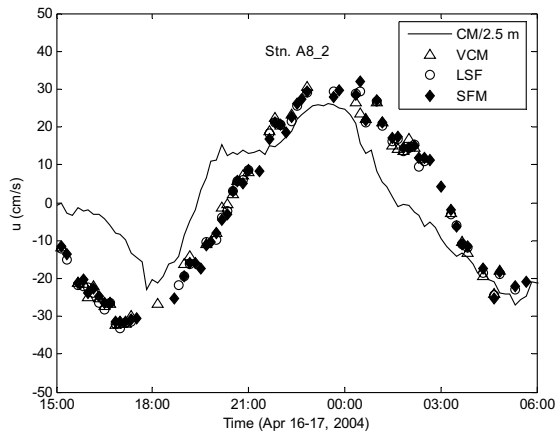


Fig. 13. Plots of the eastward (u) and northward (v) components of HF radar by VCM, LSF and SFM and current meter currents, along with the RMS differences noted. (a) At mooring station A8_1; (b) At mooring station A2; (c) At mooring station A8_2.

In-situ current measurements were provided by an Aanderaa current meter lowered from the ship at each station, which recorded current magnitude and direction at three depths: 1.5, 2.0 and 2.5 m. Unfortunately, the direction sensor of the current meter installed at 2.5 m depth was not working correctly from the first day's mooring at A8 (A8_1) to the morning of April 16. Furthermore, only the direction sensor at 2.5 m depth was working well when the ship moored at station A8 again (A8_2) at the last time period during the experiment. The current magnitude sensors at three depths were always working correctly.

Continuous observations were conducted at mooring locations A8_1, A2, and A8_2 each for about 14 hours during the experiment. Here, a comparison is presented between the vector current velocities measured by the dual-site OSMAR systems and those measured effectively by current meters moored at three depths of 1.5, 2.0 and

2.5 m for those three locations, taking account of the difference in measuring depths and the effect of the spatial variation of current within the radar target cell (Steward and Joy, 1974). Graphs of the eastward (u) and northward (v) currents produced by VCM, LSF and SFM versus the current meter eastward and northward current at different depths at above three locations are shown in Fig. 13. There is good agreement between radar measurements and current meter measurements. In the current maps, A2 was located in the marginal area of dual-site radar common coverage, so radials from the two radars could not be obtained simultaneously when the sea echoes were absent or weak. Figure 13(b) illustrates that VCM and LSF currents were not generated sometimes, while SFM currents consistent with current meter measurements were produced during the whole observation time. Taking into account the bias of the radars' radial measurements, it is thought that SFM results from a single-site radar data were



(c)

Fig. 13. (continued).

generally rational.

Because of the 2-D movement of water particles in the ocean surface waves, the radial current velocity measured by HF radar generally corresponds to a value averaged between the surface and a certain depth. Steward and Joy (1974) showed that the “effective” depth of surface current detected by HF radar was related to the radar frequency. Under the linear-current-profile assumption, the “effective” depth of OSMAR measurements was about 1.5 m. A vector current map was output every 10 minutes for radar measurements, while current meter measurements were recorded each 2 minutes. Current meter records were averaged each 10 minutes, which is convenient for comparison. Figure 14 shows scatter diagrams of the current velocities measured by OSMAR for three methods versus those measured by current meter at 1.5 m depth. The correlation between SFM results and current meter is highest, about 48.1%; the slope of the linear least-square fit to the data comes to a maximum 0.609, too.

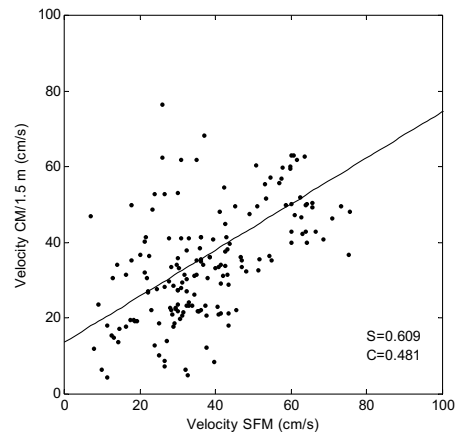
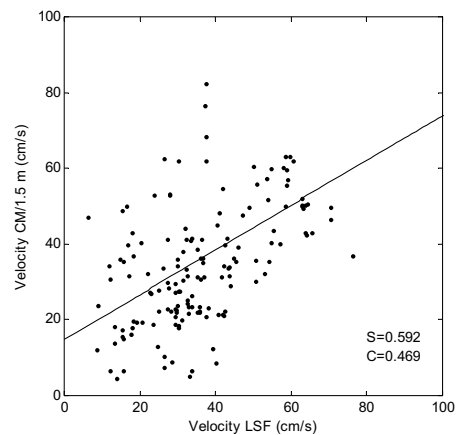
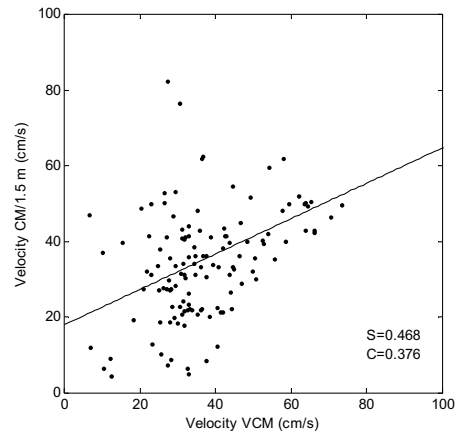


Fig. 14. Scatter diagrams of the current velocities of HF radar by VCM, LSF, SFM and current meter currents at 1.5 m depth. The correlation coefficient R and slope S of the linear fit between HF radar and current meter currents are noted.

The total currents of radar algorithms are compared with current meter measurements; the statistics of RMS errors of the eastward component and northward component are listed in Table 5. There are great differences be-

Table 5. RMS errors of currents by HF radar algorithms compared with current meter measurements at different depths.

Depth (m)	u_{rms} (cm/s)			v_{rms} (cm/s)		
	VCM	LSF	SFM	VCM	LSF	SFM
1.5	11.2	10.1	10.5	14.4	15.3	12.2
2.0	11.9	11.2	10.0	13.6	14.7	11.7
2.5	16.7	15.6	15.6	13.8	15.1	14.7

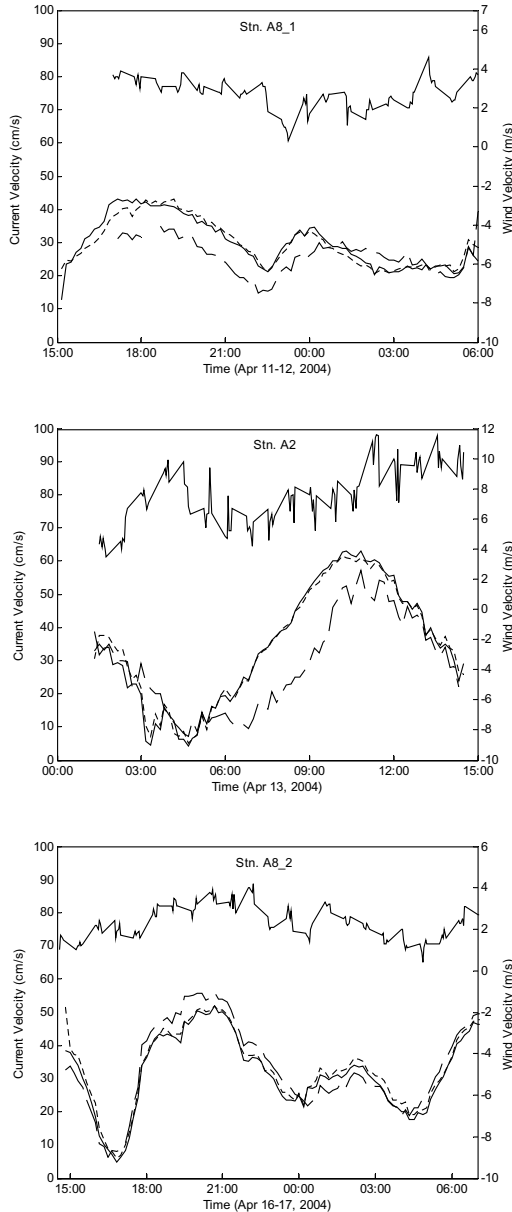


Fig. 15. Time series of wind velocities at 10 m altitude (upper solid lines) versus current velocities measured by the current meters at three depths: the solid lines show current velocities at a depth of 1.5 m; the short-dashed lines show current velocities at a depth of 2.0 m; the long-dashed lines show current velocities at a depth of 2.5 m.

tween the currents measured by the HF radar and by the current meter. This is thought to be connected with the differences of two measurement means besides the radial observation errors. Current meters effectively measure current at a single point in a certain depth while the radar measurements represent an average over an area of about 6.25 km² and a depth of 1–2 m, so the two instruments do not survey exactly the same area.

4.4 Vertical shear: Relationship to wind

It is observed that the slopes in Fig. 14 are all less than 1, which indicates that radar measurements are inclined to be larger than current meter measurements. We find a positive difference statistically by comparing the current velocity measured by the radar and the 1.5-m current meter. It is thought that vertical shear of horizontal velocities existed in the surface layer, presumably due to wind stress on the sea surface.

Wind speed and direction at 10 m altitudes were obtained using a XZC5-1 shipping telemetry system at each mooring station during the experiment. Wind measurements were recorded for 15 minutes every 45 minutes. Figure 15 shows time series of wind velocity at 10 m altitude and current velocities measured by the current meters at three stations. When the ship was moored at Station A2, there was a relatively strong wind with velocity of about 6–12 m/s. Figure 15(b) indicates an obvious shear, but it does not seem to be directly related to the wind velocity. We argue that the M2 tidal current dominates in the study region, but the total current includes a tidal component and a wind-driven one, both of which may vary with depth. To get a better estimate of the wind-driven component, the tidal component should be subtracted from the total. Due to the limited field data, the tidal component could not be filtered out. Further discussion of the vertical shear as well as the correlation of the direction of the current with respect to the wind will therefore be postponed until we obtain more observations.

5. Conclusions

Traditionally, the vectorial current combination (VCM) or least-squares fitting (LSF) algorithm is applied to obtain vector fields when two (or more) HF-SWRs are available. Here we propose a new algorithm, the stream

function method (SFM), for providing total current maps from dual-site HF radar radials. The new algorithm avoids the errors of the VCM due to linear interpolation of vector current maps in combination in a grid of longitude-latitude cells and has the advantage over the LSF in recovering a complicated current field. The new method can also generate vector current maps over a larger radar coverage area.

We first evaluate the performance of SFM, compared with the other two in simulation. Three factors are examined: the effect of radial current errors, the effect of currents' spatial variation, and the response to horizontal divergence. Compared with VCM and LSF, SFM has two main advantages: 1) SFM has better acceptance of radial errors and is more robust in processing the complicated current fields. 2) SFM current maps cover a larger sea area. It also indicates that SFM is applicable to single-site radar measurements. The performance of SFM will not be significantly affected by a horizontal divergence unless it is very large, up to $10^{-5}/s$, but so large a divergence is seldom observed in the study region, or in most of the world's oceans.

SFM is tested on OSMAR real data collected at the coastal East China Sea in April, 2004. The experiment data demonstrate the validity of SFM. The performance of SFM is very similar to LSF in the common coverage area. However, realistic currents are generated using SFM in the marginal area only illuminated by one radar, where vector currents cannot be combined using VCM and LSF. The currents maps produced by the three methods indicate that the direction of vector field rotates clockwise, due to a dominant tidal current component. Compared with *in-situ* current data measured by 1.5-m current meters, the correlation of current velocity between SFM results and current meter measurements is highest, about 0.481, and the slope of the linear least-square fit to the data comes to a maximum 0.609, too. The RMS difference of SFM results is smaller than that of VCM and LSF results, compared with current meter observations at all three depths. Preliminary analysis of the vertical current shear is conducted based on the current meter and wind measurements.

Improving the HF radar radial current measurement accuracy, especially the direction of arrival (DOA) techniques, has been demonstrated to influence the performance of SFM. Horizontal divergence will be tied to computational accuracy of SFM, and the application of numerical current model appropriate for divergent flow will be studied in future work. Another topic of future work is the investigation of the applications of SFM in single-site HF radar vector current measurements.

Acknowledgements

This work is supported by the National Natural Sci-

ence Foundation of China under Grant 60571065, 60201003 and 40406020, and the 863 High Technology Program of China under Grant 2004AA604080.

References

- Barrick, D. E. (1972): First order theory and analysis of MF/HF/VHF scatter from the sea. *IEEE Trans. Antennas Propagat.*, **20**(1), 2–10.
- Barrick, D. E., M. W. Evans and B. L. Weber (1977): Ocean surface currents mapped by radar. *Science*, **198**, 138–144.
- Guo, X. and T. Yanagi (1998): Three-dimensional structure of tidal current in the East China Sea and the Yellow Sea. *J. Oceanogr.*, **54**(6), 651–668.
- Huang, Z., G. Yu *et al.* (1996): Numerical modeling of tide-induced upwelling in the coastal areas of the East China Sea. *Journal of Ocean University of Qingdao*, **4**, 405–412 (in Chinese).
- Kang, Y. Q. (1984): An analytic model of wind-driven current in the Yellow, the East China and the South China Seas. p. 143–154. In *Ocean Hydrodynamic of the Japan and East China Seas*, ed. by Ichiye, Elsevier Science Publishers, Netherlands.
- Kesan, C. (2003): Taylor polynomial solutions of linear differential equations. *Applied Mathematics and Computation*, **142**(1), 155–165.
- Kowalik, Z. and T. S. Murty (1993): *Numerical Modeling of Ocean Dynamics*. World Scientific Publishing, Singapore, p. 319–332.
- Leise, J. A. (1984): The analysis and digital signal processing of NOAA's surface current mapping system. *IEEE J. Oceanic Eng.*, **9**(2), 106–113.
- Lewis, J. K., I. Shulman and A. F. Blumberg (1998): Assimilation of Doppler radar current data into numerical ocean models. *Cont. Shelf Res.*, **18**, 541–559.
- Lipa, B. J. and D. E. Barrick (1983): Least-Squares methods for the extraction of surface currents from CODAR crossed-loop data: application at ARSLOE. *IEEE J. Oceanic Eng.*, **8**(4), 226–253.
- Lipphardt, B. L., A. D. Kirwan and C. E. Grosch (2000): Blending HF radar and model velocities in Monterey Bay through normal mode analysis. *J. Geophys. Res.*, **105**(C2), 3425–3450.
- Luo, Y. and G. Yu (1998): Numerical studies of wind- and TWC-driven upwelling in coastal areas of the East China Sea. *Journal of Ocean University of Qingdao*, **28**(4), 536–542 (in Chinese).
- Nadai, A., H. Kuroiwa, M. Mizutori and S. Sakai (1997): Measurement of ocean surface currents by the CRL HF ocean surface radar of FMCW type. Part 1. Radial current velocity. *J. Oceanogr.*, **54**(4), 325–342.
- Nadai, A., H. Kuroiwa, M. Mizutori and S. Sakai (1999): Measurement of ocean surface currents by the CRL HF ocean surface radar of FMCW type. Part 2. Current vector. *J. Oceanogr.*, **55**(1), 13–30.
- Oke, P. R., J. S. Allen, R. N. Miller, G. D. Egbert and P. M. Kosro (2002): Assimilation of surface velocity data into a primitive equation. *J. Geophys. Res.*, **107**(C9), 3122, doi:10.1029/2000JC000511.

- Paduan, J. and I. Shulman (2004): HF radar data assimilation in the Monterey Bay area. *J. Geophys. Res.*, **109**(CO7S09), doi:10.1029/2003JC001949.
- Pang, C., D. Hu *et al.* (2002): A method of evaluating upwelling velocity. *Marine Science*, **26**(8), 67–71 (in Chinese).
- Stewart, R. H. and J. W. Joy (1974): HF radio measurement of surface currents. *Deep-Sea Res.*, **21**, 1039–1049.
- Teague, C. C., G. L. Tyler and R. H. Steward (1977): Studies of the sea using HF radio scatter. *IEEE Trans. Antennas Propagat.*, **25**, 12–19.
- Yang, S. and H. Ke *et al.* (2001): Super-resolution ocean surface current based on MUSIC for OSMAR2000. *IEEE Conference and Exhibition*, **2**, 930–941.
- Zhu, J., P. Ding and D. Hu (2003): Observation of the diluted water and plume front off the Changjiang River estuary during August 2000. *Oceanologia Et Limnologia Sinica*, **34**(3), 249–255 (in Chinese).